

SINGLE HIGGS-BOSON PRODUCTION THROUGH  $\gamma\gamma$  SCATTERING  
WITHIN THE GENERAL 2HDM

**Nicolás Bernal, David López-Val, Joan Solà**

*High Energy Physics Group, Dept. ECM, and Institut de Ciències del Cosmos  
Univ. de Barcelona, Av. Diagonal 647, E-08028 Barcelona, Catalonia, Spain*

E-mails: bernal@ecm.ub.es, dlopez@ecm.ub.es, sola@ecm.ub.es.

***Abstract.*** The production of a single neutral Higgs boson  $h$  through (loop-induced)  $\gamma\gamma$  collisions is explored in the context of the linear colliders within the general Two-Higgs-Doublet Model (2HDM). Two different mechanisms are analyzed: on the one hand, the scattering  $\gamma\gamma \rightarrow h$  of two real photons in a  $\gamma\gamma$  collider; on the other, the more traditional mechanism of virtual photon fusion,  $e^+e^- \rightarrow e^+e^-\gamma^*\gamma^* \rightarrow e^+e^- + h$ . Owing to the peculiar properties of the Higgs boson self-interactions within the general 2HDM, we find that the overall production rates can be boosted up significantly, provided the charged Higgs mass is not too heavy. For example, if  $M_{H^\pm} \gtrsim 100 \text{ GeV}$  and, in addition,  $M_{h^0}$  falls in the ballpark of the LEP bound on the SM Higgs mass up to a few hundred GeV, the cross-sections may typically render  $\langle\sigma_{\gamma\gamma \rightarrow h}\rangle \sim 0.1 - 1 \text{ pb}$  and  $\sigma(e^+e^- \rightarrow e^+e^-h^0) \lesssim 0.01 \text{ pb}$  – in both cases well above the SM prediction. Although for  $M_{H^\pm} > 300 \text{ GeV}$  the rates become virtually insensitive to the Higgs boson self-couplings, a significant tail of non-SM effects produced by the combined contribution of the Yukawa couplings and gauge bosons could still reveal a smoking gun.

# 1 Introduction

The Higgs mechanism is the most fundamental lingering issue that remains experimentally unsettled in Particle Physics. It is difficult to overemphasize that this issue stands right in the core of our present understanding of the Standard Model (SM). For one thing is the only known strategy to build up a (perturbative) renormalizable quantum field theoretical description of Electroweak Symmetry Breaking (EWSB). It means that, to a great extent, it embodies the backbone of the SM structure.

The central assumption here is the existence of (at least) one elementary spinless field – the so-called Higgs boson. Its relevance is particularly evident if we take into account that the presence of (at least) one such field in the structure of the model is indispensable for the unitarity of the theory. If no Higgs bosons exist below the TeV scale, weak interactions would actually become strong at that scale and e.g. the  $WW$  cross-section would violate the unitarity of the scattering matrix. Moreover, in the absence of Higgs bosons the various particle masses could not be generated consistently (i.e. without spoiling the ultraviolet behavior of the theory at higher orders of perturbation theory). In short, if no Higgs bosons are there to protect the (presumed) perturbative structure of the weak interactions, the latter would enter a perilous runaway regime at high energies. It is, thus, essential to confirm experimentally the existence of one or more Higgs particles through their explicit production in the colliders.

Apart from the single neutral (CP-even) Higgs boson  $H$  of the SM, other opportunities may arise in model building that could serve equally well the aforementioned purposes. Perhaps the most paradigmatic extension of the SM is the Minimal Supersymmetric Standard Model (MSSM) [1], whose Higgs sector involves two doublets of complex scalar fields. The physical spectrum consists of two charged states,  $H^\pm$ , two neutral CP-even states  $h^0, H^0$  (with masses  $M_{h^0} < M_{H^0}$ ) and one CP-odd state  $A^0$  [2].

We shall not dwell here on the whys and wherefores of supersymmetry (SUSY) as a most sought-for realization of physics beyond the SM. It suffices to say that it provides a Higgs sector which is stable (to all orders in perturbation theory) under embeddings of the low-energy structure into a Grand Unified Theory, and in particular it provides the most natural link with gravity [1]. But, how to test the structure of the Higgs sector? In the MSSM case, such structure is highly constrained by the underlying supersymmetry. As a consequence, the self-interactions of the SUSY Higgs bosons are rather inconspicuous, in the sense that they cannot be enhanced as compared to the ordinary gauge interactions and, therefore, do not present a very distinctive phenomenology. The bulk of the enhancing capabilities of the MSSM Lagrangian resides, instead, in the rich structure of Yukawa couplings between Higgs bosons and quarks or between quarks, squarks and chargino-neutralinos. The stupendous phenomenological opportunities associated to these supersymmetric structures are well-known since long ago (cf. [3, 4]) and have been continuously updated in the literature (for recent reviews, see e.g. [5]).

On the other hand, we should be prepared for alternative forms of Higgs boson physics of a more generic kind, whose potential implications can be equally outstanding and nevertheless be concentrated on very different sectors of the model. This could e.g. be the case of the general (unconstrained) Two-Higgs-Doublet Model (2HDM), where again two doublets of complex scalar fields are introduced, leading to a similar physical spectrum  $h^0, H^0, A^0, H^\pm$ , but without being subdued by the severe restrictions enforced by the supersymmetric transformations. The result is a Higgs potential with a collection of Higgs boson self-interactions which, in contrast to the SUSY case, can be highly enhanced in comparison to the gauge couplings. Both the general 2HDM and the Higgs sector of the MSSM can mimic the Higgs phenomenology of the SM (e.g. in the respective decoupling limits of these models) but at the same time can present very different properties in other regimes. We refer the reader to Ref. [2, 5] for further details, and in particular

to the recent works [6] and [7] for some outstanding and distinctive phenomenological consequences of the generic 2HDM Higgs boson self-couplings at the colliders.

Let us assume that the LHC unveils a neutral Higgs boson. At that point, the crucial question will be to make sure that the new particle is really what is supposed to be. Actually, an essential part of the very process of identification will be to disclose just whether such particle is actually the neutral SM Higgs boson, a neutral member of a SUSY extension of the SM (typically the MSSM), or rather a generic neutral Higgs boson of a non-SUSY alternative setup, such as e.g. the general 2HDM. Undoubtedly, an operational criterion to ferret out the nature of the potential newcomer will be to observe the concomitant phenomenological properties that gives rise to. Unfortunately, this is sooner said than done; for example, this will not be a completely trivial task at the LHC due to the manifold and powerful sources of background there [5]. In this sense, the complementary help of the future linear  $e^+e^-$  colliders (linac) [8], such as the ILC and CLIC, can play a momentous role to unravel the ultimate nature of the purported Higgs boson scalar particle(s) presumably produced at the LHC. The reason is clear: we need to perform precise measurements of the Higgs boson properties and a linear collider is the cleanest large-scale instrument we may think of for precision physics. There are many studies in the literature supporting this fact. For instance, the trilinear (3H) couplings have been investigated phenomenologically in TeV-class linear colliders in [9–12] through the double-Higgs strahlung process  $e^+e^- \rightarrow \text{HHZ}$  or the WW double-Higgs fusion mechanism  $e^+e^- \rightarrow \text{H}^+\text{H}^-\nu_e\bar{\nu}_e$ . These processes, which include vertices like ZZH, WWH, ZZHH, WWHH and HHH, are possible both in the SM and its extensions, such as the MSSM and the general 2HDM. Unfortunately, the cross-section turns out to be rather small both in the SM and in the MSSM, being of order of 1 fb [9]. Even worse is the situation regarding the 3H boson production in the MSSM, in which the typical cross-sections just border the value  $\sim 0.01$  fb or less – except in the case of some particular resonant configuration [9]. Quite in contrast to these meager MSSM expectations, it has recently been shown that the general 2HDM can provide cross-sections two to three orders of magnitude larger within the same experimental setup [6, 7].

Closely connected to the physics of the linear colliders will be the physics of the  $\gamma\gamma$  colliders [13]. As is well-known, a collider of this sort can be optionally realized from a linac if an intense laser pulse is flushed onto the lepton beams and made to collide about one mm in front of the interaction point. By the process of backward Compton scattering between the laser photons and the linac leptons, the laser pulse is converted into a highly energetic photon beam. The upshot is that one may obtain beams of photons with an amplified energy very near the original  $e^+e^-$  energy and a luminosity that is of the same order as that of the primary linac beams in the high energy part of the spectrum. In other words, a high-energy  $\gamma\gamma$  collider can be put at work out of essentially the same technology needed to construct a linac. The outcome is one of the nicest, cleanest and most sophisticated machines ever to be constructed in high energy physics for precision experiments. Not surprisingly, a  $\gamma\gamma$  collider should enable us to probe the most sensitive theoretical structures of gauge theories, and certainly the Higgs sector is a most preeminent one.

Currently, a renewed thrust of theoretical activity has been invested in double Higgs production in  $\gamma\gamma$  collisions within the general 2HDM [14] – see also [15, 16] for earlier related work and [17] for single and double Higgs production in the SM and the MSSM. In this Letter, and following the spirit of the recent works [6, 7], we wish to further explore the Higgs boson self-interactions in the general 2HDM by focusing on the process of single neutral Higgs boson production  $\gamma\gamma \rightarrow h = h^0, H^0, A^0$  in the context of both  $\gamma\gamma$  real scattering and  $\gamma\gamma$  virtual fusion in  $e^+e^-$  colliders (see Fig. 1).

## 2 Loop-induced $\gamma\gamma h$ interactions within the 2HDM: general features and computational setup

Let us recall that the general 2HDM [2] is obtained by canonically extending the SM Higgs sector with a second  $SU_L(2)$  doublet carrying weak hypercharge  $Y = +1$ , so that it contains 4 complex scalar fields. The free parameters in the most general, CP-conserving, 2HDM potential can be expressed in terms of the masses of the physical Higgs particles,  $M_{h^0}$ ,  $M_{H^0}$ ,  $M_{A^0}$ ,  $M_{H^\pm}$ , the ratio  $\tan\beta = v_2/v_1$  of the two VEV's giving masses to the up- and down-like quarks, the mixing angle  $\alpha$  between the two CP-even states, and, finally, the coupling  $\lambda_5$  which cannot be absorbed in any of the previous quantities<sup>1</sup>. In turn, the possible 2HDM coupling patterns in the Higgs-fermion sector are commonly sorted out as follows: i) type-I models, in which only one Higgs doublet couples to fermions, whereas the other doublet does not; and ii) type-II models, wherein a doublet couples only to down-like fermions and the other doublet only to up-like fermions. In either way one may avoid the appearance of dangerous (tree-level) Flavor Changing Neutral Current (FCNC) processes [2]. The MSSM Higgs sector is actually a type-II one, but of a very restricted sort (enforced by SUSY invariance) [1].

On top of that a number of important restrictions, emerging from either the available experimental data and the theoretical consistency of the model, must be taken into account in order to obtain a more realistic output. Although we have already described these constraints in [6, 7] (see also [18]), we will introduce some qualifications here. To start with, there are (additional) stringent constraints coming from (one-loop induced) low-energy FCNC processes, mainly from the charged Higgs boson contributions to  $\mathcal{B}(b \rightarrow s\gamma)$  [19], which require  $M_{H^\pm} > 295 \text{ GeV}$  (for  $\tan\beta \geq 1$ ) in type-II models. Let us emphasize that this bound does not apply to type-I models since for them the charged Higgs couplings to fermions are proportional to  $\cot\beta$  and hence the loop contributions are highly suppressed at large  $\tan\beta$ . Furthermore, the approximate  $SU(2)$  custodial symmetry severely restricts the radiative corrections to the  $\rho$  parameter from the 2HDM degrees of freedom; experimentally  $|\delta\rho| \leq 10^{-3}$  [20]. Moreover, there are of course the bounds stemming from the unsuccessful Higgs boson searches at LEP and the Tevatron [20]. Besides, a very important set of conditions emerges from the unitarity constraints. A substantial number of studies are devoted to this subject in the literature [21, 22], although their conclusions are not always fully coincident. Alternatively, one can stick to a less restrictive (albeit well-motivated) framework based on requiring that none of the triple and quartic Higgs boson self-couplings (in the mass-eigenstate basis) should be larger than the upper value of the corresponding couplings in the SM. Ultimately, this condition is grounded on the Lee-Quigg-Thacker unitarity bound [23] on the SM Higgs boson mass. In this way, we obtain a double set of conditions that significantly harness the size of the 3H and 4H couplings in the 2HDM:

$$|C_{hhh}| \leq \left| \lambda_{HHH}^{(SM)}(M_H \simeq 1 \text{ TeV}) \right| = \frac{3 e M_H^2}{2 \sin\theta_W M_W} \Big|_{M_H=1 \text{ TeV}}, \quad (1)$$

$$|C_{hhhh}| \leq \left| \lambda_{HHHH}^{(SM)}(M_H \simeq 1 \text{ TeV}) \right| = \frac{3 e^2 M_H^2}{4 \sin^2\theta_W M_W^2} \Big|_{M_H=1 \text{ TeV}} \quad (2)$$

( $-e$  being the electron charge and  $\theta_W$  the weak mixing angle). In the following, we will discuss our results by taking into account the conditions (1) and (2), and we will briefly compare them with the restrictions derived in Ref. [21]. Furthermore, we shall impose that the EW vacuum is stable,

---

<sup>1</sup>Throughout the paper, we use the notation and conventions of Ref. [6], to which we refer the reader for further details. Here, in contrast to that reference, we leave  $\lambda_5$  as a fully independent parameter.

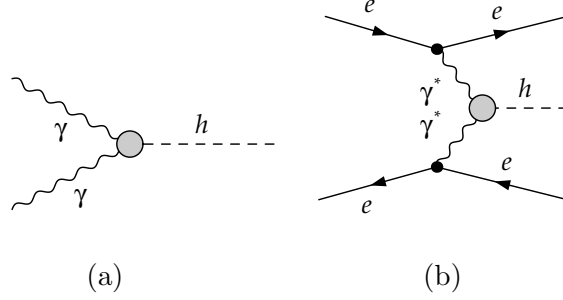


Figure 1: Generic Feynman diagrams describing the single Higgs production process through the mechanisms of a) direct scattering of a real photon pair and b) virtual  $\gamma\gamma$  fusion in  $e^+e^-$  collisions. The grey blobs stand for the generic loop-induced  $\gamma\gamma h$  interaction at any order in perturbation theory.

which is tantamount to say that we demand the quartic interaction terms in the potential not to give negative contributions producing an unbounded potential from below [24]. This condition leads to

$$\Lambda_1 > 0, \quad \Lambda_2 > 0, \quad \sqrt{\Lambda_1 \Lambda_2} + \Lambda_3 + \text{Min}(0, \Lambda_4 + \Lambda_5, \Lambda_4 - \Lambda_5) > 0, \quad (3)$$

where the parameters  $\Lambda_i$  are defined in terms of the  $\lambda_i$  ones [6] as follows:

$$\begin{aligned} \Lambda_1 &= 2(\lambda_1 + \lambda_3), & \Lambda_2 &= 2(\lambda_2 + \lambda_3), & \Lambda_3 &= 2\lambda_3 + \lambda_4, \\ \Lambda_4 &= -\lambda_4 + \frac{1}{2}(\lambda_5 + \lambda_6), & \Lambda_5 &= \frac{1}{2}(\lambda_5 - \lambda_6). \end{aligned} \quad (4)$$

In this Letter, we are concerned with the production of a Higgs-boson via  $\gamma\gamma$  scattering. This process can proceed through the following two basic and independent mechanisms:

- Direct scattering of two real photons  $\gamma\gamma \rightarrow h$ , see Fig. 1a;
- Virtual two-photon fusion in  $e^+e^-$  collisions, namely  $e^+e^- \rightarrow e^+e^-\gamma^*\gamma^* \rightarrow e^+e^- + h$  (Fig. 1b).

Although a tree-level  $\gamma\gamma h$ -coupling is not allowed by the electromagnetic gauge symmetry, this interaction is generated at the quantum level through a plethora of radiative corrections, whose description in terms of Feynman diagrams is displayed in Figure 2. The entire set of diagrams corresponds to the production process  $\gamma\gamma \rightarrow h$  for both CP-even states  $h = h^0, H^0$ , whereas for the production of the CP-odd one,  $\gamma\gamma \rightarrow A^0$ , only the first line of diagrams is allowed (owing to C and CP-invariance). On the other hand, Lorentz invariance dictates the general structure of the effective  $VVh$  coupling:

$$\Gamma_{\mu\nu} = F_1 g_{\mu\nu} + F_2 (p_{1\mu} p_{2\nu} - g_{\mu\nu} p_1 p_2) + i F_3 \epsilon^{\rho\sigma}_{\mu\nu} p_{1\rho} p_{2\sigma}, \quad (5)$$

where  $F_{1,2,3}$  are the corresponding form factors, which are in general functions of the incoming momenta  $p_1$  and  $p_2$  of the photons. The scattering amplitude is

$$\mathcal{M}_{\eta_1, \eta_2}(\gamma\gamma \rightarrow h) = \epsilon^\mu(p_1, \eta_1) \epsilon^\nu(p_2, \eta_2) \Gamma_{\mu\nu}, \quad (6)$$

where  $\epsilon^\mu(p_1, \eta_1)$  and  $\epsilon^\nu(p_2, \eta_2)$  are the polarization four-vectors of the two photons. The corresponding cross-section can be written

$$\sigma(\gamma\gamma \rightarrow h) = \frac{\pi}{M_h^2} |\mathcal{M}_{\eta_1, \eta_2}(\gamma\gamma \rightarrow h)|^2 \delta(s - M_h^2). \quad (7)$$

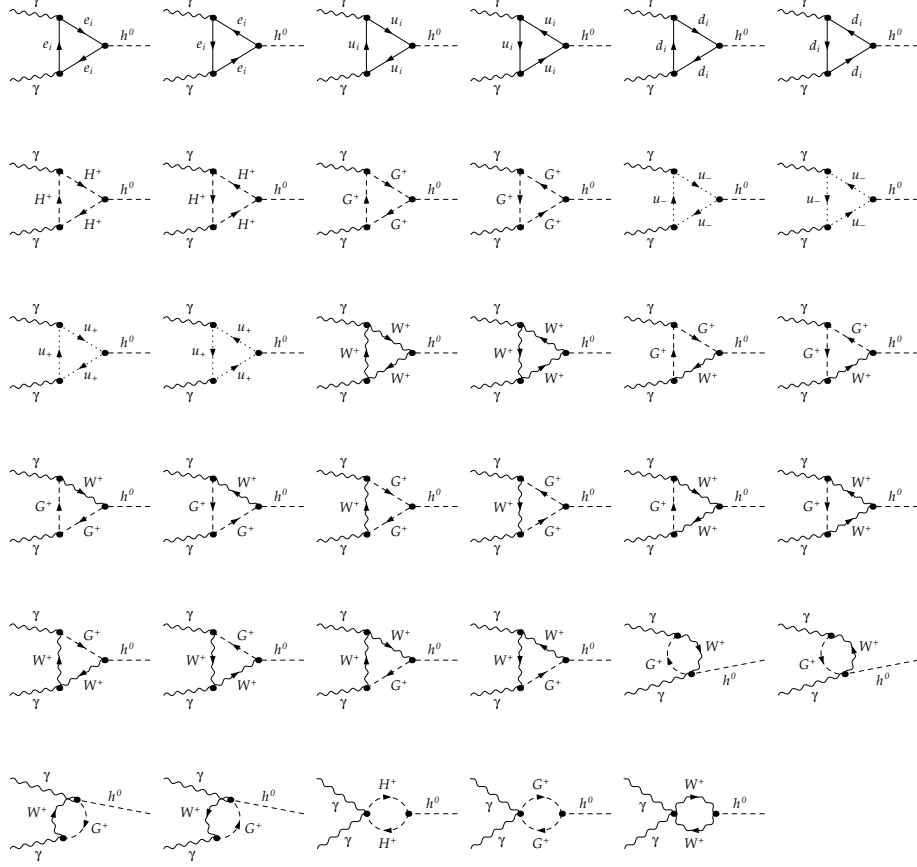


Figure 2: Feynman diagrams describing the process  $\gamma\gamma \rightarrow h^0$ , at the one-loop level, within the 2HDM. In the SM case, we have to disregard the diagrams with charged Higgs bosons.

The presence of a Dirac delta, which is a trademark feature of the  $2 \rightarrow 1$  phase space, implies that this cross-section is properly defined only as a distribution. In practice, we can handle this conveniently by rewriting Eq. (7) with the replacement

$$\delta(s - M_h^2) \rightarrow \frac{1}{\pi} \frac{s \Gamma_h / M_h}{(s - M_h^2)^2 + (s \Gamma_h / M_h)^2}, \quad (8)$$

$\Gamma_h \equiv \Gamma(h \rightarrow \text{all})$  here being the total Higgs boson decay width, assumed to be much smaller than  $M_h$ . Alternatively, one can express the final result in terms of the partial width of the decay  $h \rightarrow \gamma\gamma$  as follows:

$$\sigma(\gamma\gamma \rightarrow h) = \frac{8\pi^2}{M_h} \Gamma(h \rightarrow \gamma\gamma) \delta(s - M_h^2) (1 + \eta_1 \eta_2) = 8\pi \frac{\Gamma(h \rightarrow \gamma\gamma) \Gamma_h (1 + \eta_1 \eta_2)}{(s - M_h^2)^2 + M_h^2 \Gamma_h^2}, \quad (9)$$

with  $\eta_{1,2} = \pm 1$  the helicities of the two colliding photons. Following the above strategy, and computing the diagrams contributing to the amplitude with the help of the computational packages *FeynArts*, *FormCalc* and *LoopTools* [25], we may finally arrive at the  $\gamma\gamma$ -induced single Higgs boson cross-section. In order to obtain more accurate results, a running value for the electromagnetic coupling constant  $\alpha_{em}(M_Z) = 1/127.9$  has been used.

### 3 Single Higgs boson production in a $\gamma\gamma$ collider

As sketched in the introduction, the basic  $\gamma\gamma$  collider operates mainly through the mechanism of Compton (back)scattering of laser photons off the linac beams [13]. In a nutshell: a photon from a laser pulse collides with a high energy electron (or positron) at a small angle; as a result, the electron recoils and one is left with a Compton-scattered photon traveling in the direction of the original incident electron. The efficiency of the  $e^\pm \rightarrow \gamma$  “conversion” will depend on many factors, such as the energy of each of the beams, the properties of the laser as well as on several non-linear effects and subleading mechanisms which turn out to modulate the overall process. As a matter of fact, the entire procedure comes down to furnish a  $\gamma\gamma$  luminosity spectrum, for which several standard parameterizations are available. This spectrum is essential to compute the expected number of events (in our case the number of produced Higgs bosons of a particular neutral species  $h = h^0, H^0, A^0$ ). To this end, the cross-section computed in the previous section must be appropriately folded with the normalized (dimensionless) photon densities provided by the given parameterizations. The total (unpolarized)  $\gamma\gamma$  cross-section, after  $e^\pm \rightarrow \gamma$  “conversion” of the primary linac beam, can finally be engineered from the following recipe:

$$\langle \sigma_{\gamma\gamma \rightarrow h} \rangle(s) = \sum_{\{ij\}} \int_0^1 d\tau \frac{d\mathcal{L}_{ij}^{ee}}{d\tau} \hat{\sigma}_{\eta_i \eta_j}(\hat{s}), \quad (10)$$

where the partonic cross-section  $\hat{\sigma}_{\eta_i \eta_j}$  is given by Eqs. (7)-(8)/(9) with  $s \rightarrow \hat{s} = \tau s$  ( $s$  in the last expression being the CM energy of the primary linac machine):

$$\hat{\sigma}_{\eta_i \eta_j}(\hat{s}) = \frac{\Gamma_h}{M_h} \frac{|\mathcal{M}_{\eta_i \eta_j}(\gamma\gamma \rightarrow h)|^2}{(\hat{s} - M_h^2)^2 + M_h^2 \Gamma_h^2}. \quad (11)$$

In the above expression,  $d\mathcal{L}_{ij}^{ee}/d\tau$  stands for the (differential) photon luminosity distribution constructed out of the photon densities  $f_{j/e_1}, f_{i/e_2}$  as follows:

$$\frac{d\mathcal{L}_{ij}^{ee}}{d\tau} = \int_\tau^1 \frac{dx}{x} \frac{1}{1 + \delta_{ij}} [f_{i/e_1}(x) f_{j/e_2}(\tau/x) + f_{j/e_1}(x) f_{i/e_2}(\tau/x)]. \quad (12)$$

Functions  $f_{i/e_1}$  and  $f_{j/e_2}$  (one per beam of given polarization) are taken, in our case, from the standard package CompAZ [26].

In order to proceed with the numerical analysis, let us first of all examine the structure of the partonic cross-section. At fixed  $\hat{s} = M_h^2$ , it can be expressed from Eq. (9) in a simply manner:

$$\sigma(\gamma\gamma \rightarrow h) = \frac{8\pi}{M_h^2} (1 + \eta_1 \eta_2) \mathcal{B}(h \rightarrow \gamma\gamma). \quad (13)$$

If averaged over polarizations, the cross-section is given by the previous result but without the factor  $1 + \eta_1 \eta_2$ , because one has to sum over  $\eta_1, \eta_2 = \pm 1$  and divide by 4. For polarized photon beams of equal polarization (i.e.  $++$  or  $--$ ), the resulting cross-section is a factor of 2 larger. If, alternatively, we consider the case of opposite polarizations ( $+-$ ), the factor  $1 + \eta_1 \eta_2$  in (13) tells us at once that the cross-section vanishes (as expected from angular momentum conservation).

Let us emphasize that the partonic cross-section encodes already the relevant information regarding the dynamical features of the 2HDM under study. This information is obviously contained in the reduced amplitude  $\mathcal{M}$  of the effective  $h\gamma\gamma$  vertex, and thus also in the branching ratio of  $h \rightarrow \gamma\gamma$ . Notice that, in the region where the triple interaction dominates, the general behavior of that amplitude takes on the form

$$\mathcal{M}(\gamma\gamma \rightarrow h^0) \sim \frac{1}{16\pi^2} \frac{\alpha_{em} C_{H^+H^-h^0}}{M_{h^0}^2} \left[ M_{h^0}^2 \epsilon^\mu(p_1, \eta_1) \epsilon_\mu(p_2, \eta_2) - 2 \epsilon_\mu(p_1, \eta_1) p_2^\mu \epsilon_\nu(p_2, \eta_2) p_1^\nu \right]. \quad (14)$$

Obviously, in this region, the cross-section (13) is directly sensitive to the  $H^+H^-h^0$  trilinear Higgs self-interaction (cf. e.g. the first two diagrams of the second row in Fig. 2), given by

$$C_{H^+H^-h^0} = \frac{ie}{2M_W \sin \theta_W} \left[ \sin(\beta - \alpha) (M_{h^0}^2 - 2M_{H^\pm}^2) - \frac{\cos(\beta + \alpha)}{\sin 2\beta} \left( 2M_{h^0}^2 - 4\frac{1}{e^2} \lambda_5 M_W^2 \sin^2 \theta_W \right) \right]. \quad (15)$$

It follows from this expression that such coupling can be enhanced either at low or high values of  $\tan \beta$ , and also through the Higgs boson mass splittings – unlike the MSSM case. In addition, it may be heightened through its explicit dependence on the  $\lambda_5$  parameter<sup>2</sup>. Needless to say, in all cases these enhancements are strictly harnessed by the various theoretical and phenomenological constraints discussed in the previous section. By comparison, the corresponding (approximate) amplitude for the SM contribution, if we assume that is dominated by the top quark Yukawa coupling, reads:

$$\mathcal{M}(\gamma\gamma \rightarrow H) \sim \frac{1}{16\pi^2} \frac{N_c Q_t^2 \alpha_{em} e m_t^4}{M_H^4 M_W \sin \theta_W} \left[ M_H^2 \epsilon^\mu(p_1, \eta_1) \epsilon_\mu(p_2, \eta_2) - 2 \epsilon_\mu(p_1, \eta_1) p_2^\mu \epsilon_\nu(p_2, \eta_2) p_1^\nu \right]. \quad (16)$$

In the domains of the 2HDM parameter space where the 3H-coupling (15) is not overwhelming over the Yukawa and gauge boson couplings (cf. e.g. the first, third and subsequent rows of diagrams in Fig. 2), Eq. (14) does not even hold as a crude approximation. Similarly, the SM amplitude receives in general sizeable contributions from the gauge boson loops that significantly correct the estimate (16). Therefore, in general it is necessary to come to grips with the full expression for the effective coupling  $g_{\gamma\gamma h}$  (which is indeed the main object under study, mainly for the cases  $h = h^0, H^0$ ). Even more useful is to define the exact ratio between the corresponding 2HDM and SM coupling strengths at one-loop:

$$r \equiv \frac{g_{\gamma\gamma h}}{g_{\gamma\gamma H}} = \frac{|\mathcal{M}|^{2\text{HDM}}}{|\mathcal{M}|^{\text{SM}}} = \left[ \frac{\Gamma(h \rightarrow \gamma\gamma)}{\Gamma(H \rightarrow \gamma\gamma)} \right]^{1/2}. \quad (17)$$

Obviously, the 2HDM amplitude will depend on whether the model is of type-I or type-II. In the particular region where the trilinear coupling dominates for  $h^0$  production,

$$r \sim \left( \frac{M_H}{m_t} \right)^4 \left( \frac{M_W}{M_{h^0}} \right) \frac{C_{H^+H^-h^0}}{M_{h^0}}. \quad (18)$$

Warned by the previous considerations, this formula should help, if only qualitatively, to understand the physics responsible for the large enhancements from the 2HDM, specially at large  $|\lambda_5|$ , for which  $|C_{H^+H^-h^0}|/M_{h^0} \sim |\lambda_5|/e^2 \gg 1$ . To be sure, in practice we will perform the numerical analysis of the exact expression (17) and consider its behavior in general regions of parameter space.

For the sake of convenience, let us focus hereafter on the sets of Higgs boson masses displayed in Table 1 below. The mass spectrum in Set I of Table 1, for instance, allows to enhance the  $H^+H^-h^0$  coupling. Its maximum value is roughly attained for  $\sin \alpha = -0.86$ ,  $\tan \beta = 1.70$  and  $\lambda_5 = -25.0$ . Incidentally, notice that the aforementioned Set I of masses is only suitable for type-I 2HDM, due to the relatively light value chosen for the charged Higgs boson ( $M_{H^\pm} = 105$  GeV), which is below the (indirect) limit of 295 GeV afflicting the type-II models [19]. Let us recall that, experimentally, the current 95% C.L. direct mass limits for general Higgs bosons searches



2HDM	Set I	Set II	Set III	Set IV
$M_{h^0}$	115	150	200	200
$M_{H^0}$	165	200	250	250
$M_{A^0}$	100	110	290	340
$M_{H^\pm}$	105	105	300	350

Table 1: Higgs mass parameters, in GeV, used throughout the calculation.

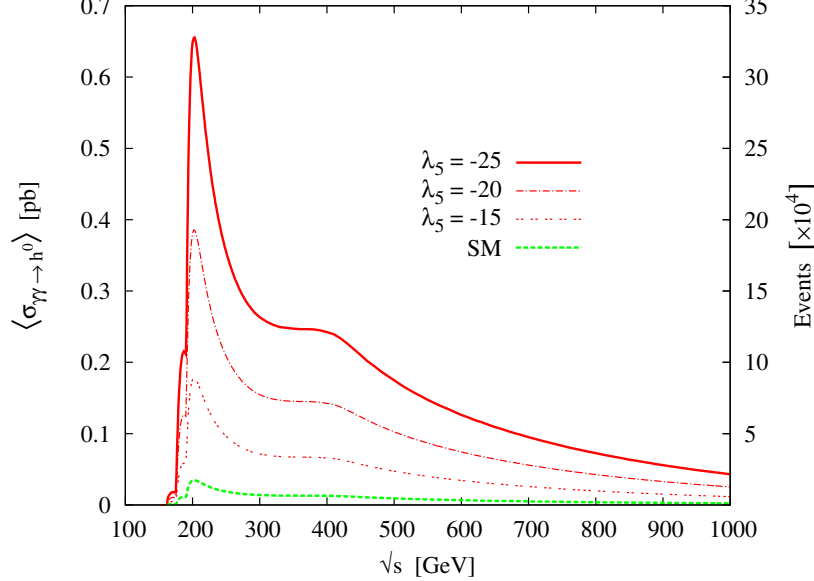


Figure 3: Cross-section  $\langle \sigma_{\gamma\gamma \rightarrow h^0} \rangle(s)$  given by Eq. (10) and number of Higgs boson events, as a function of the CM energy of the linac, assuming an (integrated) luminosity  $\mathcal{L} = 500 \text{ fb}^{-1}$ . We plot the corresponding values for the SM and the 2HDM using the Set I of Higgs boson masses,  $\sin \alpha = -0.86$ ,  $\tan \beta = 1.7$  and three values for  $\lambda_5$ .

are:  $M_{H^\pm} \gtrsim 79.3 \text{ GeV}$  for the charged Higgs boson, and  $M_{h^0} \gtrsim 92.8 \text{ GeV}$ ,  $M_{A^0} \gtrsim 93.4 \text{ GeV}$  ( $\tan \beta > 0.4$ ) for the neutral ones (of course with  $M_{H^0} > M_{h^0}$ ) [20].

In Fig. 3, we perform the numerical analysis of the averaged total cross-section  $\langle \sigma_{\gamma\gamma \rightarrow h} \rangle(s)$ , Eq. (10), in which the partonic contribution is folded with the effective luminosity function (12). We display  $\langle \sigma_{\gamma\gamma \rightarrow h} \rangle(s)$  as a function of the center-of-mass (CM) energy  $\sqrt{s}$  of the linac machine for the Set I of Higgs masses. In this figure, we explore a region of parameter space where the  $H^+H^-h^0$  coupling dominates for different negative values of  $\lambda_5$  (As we will see later on, large  $\lambda_5 > 0$  values are forbidden by vacuum stability.). Notice that, for sufficiently large  $|\lambda_5| > 10$ , the cross-sections can be considerably high (spanning the range  $0.01 - 0.2 \text{ pb}$ ) at the fiducial startup value  $\sqrt{s} = 500 \text{ GeV}$  of the ILC, and entailing at this point more than  $10^3 - 10^4$  events for the given integrated luminosity. The rates, however, decrease fast for smaller values of  $|\lambda_5|$ , the reason being the destructive interference between the charged Higgs, gauge boson and fermion loops at low values of  $|\lambda_5|$ . For example, at the same energy and for  $\lambda_5 = (-2, -5, -8)$  we obtain  $\langle \sigma_{\gamma\gamma \rightarrow h} \rangle = (2.40, 0.16, 5.50) \text{ fb}$  respectively. Clearly, there is a delicate balance in the low  $|\lambda_5|$  region which amounts to a severe depletion of the overall 2HDM cross-section. By comparison, the corresponding result in the SM, namely for the same Higgs mass ( $M_H = M_{h^0}$ ), reads  $\langle \sigma_{\gamma\gamma \rightarrow H} \rangle \simeq 11$

<sup>2</sup>We note that for  $\lambda_5 = \lambda_6 = 2\sqrt{2} G_F M_{A^0}^2 = e^2 M_{A^0}^2 / (2 \sin^2 \theta_W M_W^2)$ , Eq. (15) reduces to the corresponding result of Table 1 of Ref. [6], as it should.

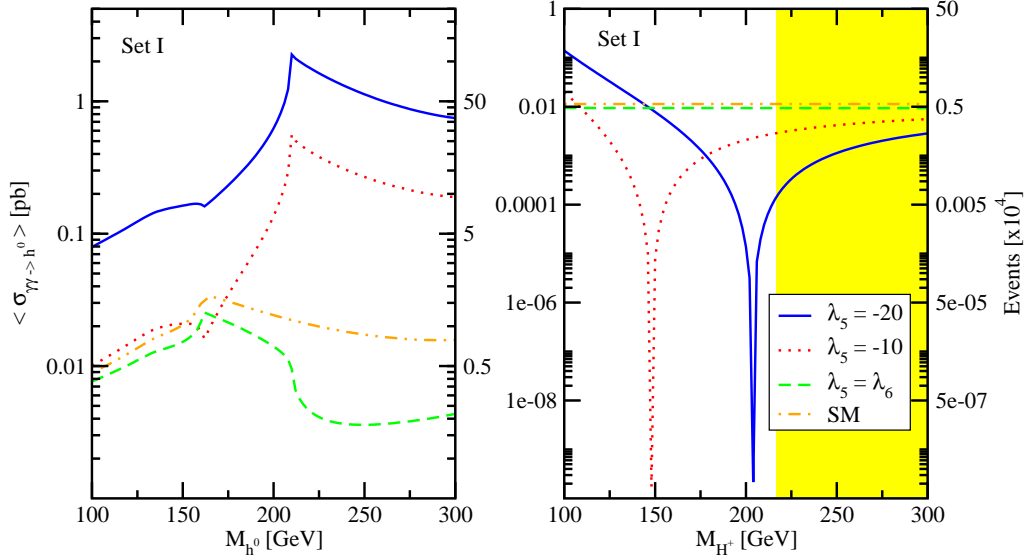


Figure 4: Cross-section  $\langle \sigma_{\gamma\gamma \rightarrow h^0} \rangle(s)$  as a function of the light CP-even Higgs mass (left panel) and the charged Higgs mass (right panel) at fixed  $\sqrt{s} = 500 \text{ GeV}$ . Remaining mass parameters from Set I,  $\sin \alpha = -0.86$ ,  $\tan \beta = 1.70$  and three values for  $\lambda_5$ :  $-20$ ,  $-10$  and  $\lambda_5 = \lambda_6$ . The SM cross-section  $\langle \sigma_{\gamma\gamma \rightarrow h^0} \rangle$  is also included (in the right panel, it almost coincides with the  $\lambda_5 = \lambda_6$  case). The shaded area is excluded by the constraints.

fb (hence  $\sim 5 \times 10^3$  events at that energy and luminosity range), which is quite sizeable. It follows that even small departures from this value should be measurable, especially in a high precision instrument as a  $\gamma\gamma$  collider.

In Fig. 4, we test the dependence of the cross-section  $\langle \sigma_{\gamma\gamma \rightarrow h^0} \rangle$  on the Higgs masses. Specifically, we plot its evolution in terms of  $M_{h^0}$  (left panel) and  $M_{H^\pm}$  (right panel). We take the other parameters from Set I while keeping  $\sin \alpha = -0.86$ ,  $\tan \beta = 1.70$ , and choose three different values for  $\lambda_5$ :  $-20$ ,  $-10$  and  $\lambda_5 = \lambda_6 = 2\sqrt{2} G_F M_{A^0}^2 \simeq 0.34$ . Included is also the SM cross-section  $\langle \sigma_{\gamma\gamma \rightarrow H} \rangle$ . Worth noticing is the fact that, while the 3H coupling is dominant, the cross-section does not immediately drop with  $M_{h^0}$ ; it actually increases for a while up to a few hundred GeV. Moreover, for large values of  $|\lambda_5|$ , the evolution of  $\langle \sigma_{\gamma\gamma \rightarrow h^0} \rangle$  presents a notorious “spike-shaped” enhancement near  $M_{h^0} \sim 2 \cdot M_{H^\pm} \sim 210 \text{ GeV}$ , which is brought about by the threshold effect of two real charged Higgs bosons in the loop. The corresponding effect for a pair of real vector bosons  $W^\pm$  at  $M_{h^0} \sim 2 \cdot M_{W^\pm} \sim 160 \text{ GeV}$  is also barely visible therein.

The sharp suppression dip standing out on the right panel of Fig. 4 deserves also a few words. Recall that, in the regime in which the influence of the trilinear contribution ( $H^+H^-h^0$ ) greatly “waxes”, the charged-Higgs mediated correction holds absolute sway over the loop-induced coupling  $g_{\gamma\gamma h^0}$ . However, as soon as we raise the charged Higgs mass, the positive influence of the trilinear Higgs boson interaction rapidly wanes and it cancels more and more against the (negative) effects from the gauge boson and fermion loops. This gives rise to the aforementioned destructive interference. Eventually, a particular value of  $M_{H^\pm}$  is reached where the two sorts of effects virtually annihilate each other (right at the vertex of the dip in the figure). Beyond this point, one rapidly reaches a regime where only the gauge boson and Yukawa coupling (negative) effects remain. Most of this region is actually excluded by the constraints. The destructive interference pattern described here is only possible when the set of Higgs boson masses is relatively light, as in the case of Set I under consideration, otherwise the trilinear effects could not be competitive.

The behavior of the effective coupling  $g_{\gamma\gamma h^0}$  in the 2HDM can be better assessed in terms of the ratio  $r$  defined in (17). Its dependence on the Higgs mass spectrum is sampled in Table 2 using

	Set I	Set II	Set III	Set IV
$r$	<b>3.98</b>	<b>3.75</b>	<b>0.98</b>	<b>0.98</b>
$\tan \beta$	1.7	1.7	1.0	1.0
$\sin \alpha$	-0.86	-0.86	-0.82	-0.82
$\lambda_5$	-25	-25	0	0

Table 2: Maximum value of the ratio  $r$ , Eq. (17), in the case of  $h^0$  and for the different mass sets quoted in Table 1, together with the configuration of  $\tan \beta$ ,  $\sin \alpha$ ,  $\lambda_5$  for which these optimal values are attained.

the parameter setups indicated in Table 1. Set II, for instance, contains a heavier neutral CP-even Higgs sector which results in a sizeable value of  $r$  of 3.75. It means that, in this case, the effective strength of the  $\gamma\gamma h^0$  vertex almost quadruples that of the SM ( $\gamma\gamma H$ ). This is quite remarkable. On the other hand, Sets III and IV are characterized by heavier charged Higgs bosons and at the same time by a heavier CP-odd Higgs bosons (so as to elude the  $\delta\rho$  bounds). Unsurprisingly, the ratio  $r$  falls in this case to within values below 1, i.e. close to the SM from below. As it should be expected, the larger the charged Higgs mass is, the less efficient is the enhancement capabilities associated to the 3H self-interactions. Incidentally, let us notice that Sets III and IV of Higgs-boson masses are intended to describe type-II 2HDM. Does this mean that for type-II models (those closer to the MSSM Higgs sector) there is no hope to hint at non-SM Higgs boson physics with  $\gamma\gamma$  collisions? Not necessarily so, as there is a tail of subleading one-loop effects triggered by the non-SM Yukawa couplings of the 2HDM in combination with the gauge bosons; in particular, we have already detected it in Fig. 4b for Set I (although within the excluded region). But, in general, this tail is available and lies well within the allowed region for heavier sets of Higgs boson masses, such as Sets III and IV. More on it below.

Figure 5 presents the corresponding contour lines for the ratio (17) in the  $(\lambda_5, \sin \alpha)$  plane. The cross symbol indicated on the left at the bottom denotes the point in this plane where such ratio attains the maximum value permitted by all the constraints. Moreover, we show the regions excluded by vacuum stability and by unitarity of the trilinear and quartic Higgs boson couplings. Notice that the sign  $\lambda_5 > 0$  is mostly forbidden by vacuum stability, which explains why we have presented the numerical analysis of the previous figures only for  $\lambda_5 < 0$ . In any case, we see that there is a sizable region left where the effective 2HDM coupling  $g_{\gamma\gamma h^0}$  is significantly larger (in fact, a few times larger) than the SM coupling  $g_{\gamma\gamma H}$ .

Finally, the available domains across the  $(\lambda_5, \sin \alpha)$  plane wherein one can obtain enhanced values of the ratio  $r$  with respect to the SM case is explored systematically in Fig. 6 for different values of  $\tan \beta$  and at the fiducial startup energy  $\sqrt{s} = 500$  GeV of the ILC. Specifically, in this figure we compute those regions in which the predicted value of the ratio  $r$  exceeds the corresponding SM value ( $r = 1$ ) by 10% at least while still being compliant with the full set of constraints; equivalently, regions where the cross-section is augmented by 20% or more, thus inducing an excess of about one thousand events above the SM prediction (within the given luminosity segment). As we can see, the projected domains are sizeable. Interestingly enough, even tiny  $\pm 1\%$  departures of  $r$  from 1 would already be significant, as they would amount to 100 events up or down the SM expectation. If we would adopt this softer criterion, the allowed domains in Fig. 6 would be substantially augmented.

Particularly stringent is the impact of the unitarity restrictions, which translates into a progressive shrinking of the relevant region as we raise the value of  $\tan \beta$ . For completeness, we have also addressed the single production of a heavy CP-even and a CP-odd Higgs boson. Their respective maximum cross-sections (at  $\sqrt{s} = 500$  GeV) for the specific case of Set I read as follows:  $\langle \sigma_{\gamma\gamma \rightarrow H^0} \rangle = 0.31$  pb and  $\langle \sigma_{\gamma\gamma \rightarrow A^0} \rangle = 1.9$  fb. The former is of the order of  $\langle \sigma_{\gamma\gamma \rightarrow h^0} \rangle$  itself, whereas

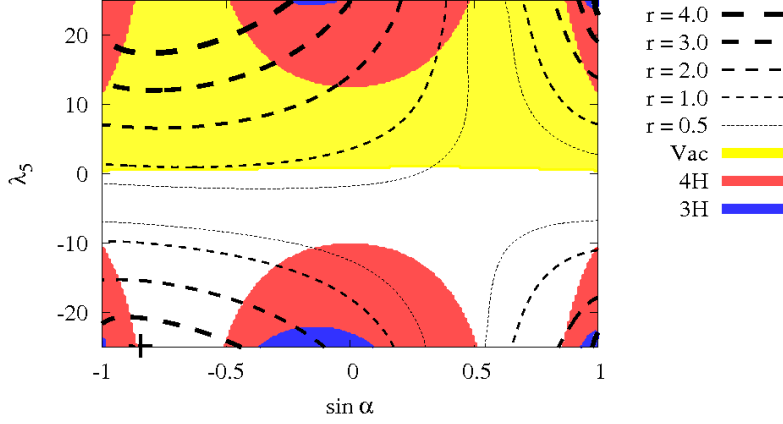


Figure 5: Contour lines for the ratio  $r = g_{\gamma\gamma h^0}/g_{\gamma\gamma H}$  (17) in the  $(\lambda_5, \sin \alpha)$  plane, for the Set I and  $\tan \beta = 1.70$ . The regions excluded by vacuum stability (upper half plane  $\lambda_5 \gtrsim 0$ ) and the unitarity of the two kinds of Higgs boson self-couplings, namely the quartic (large circular domains) and the trilinear (small circular domains), are separately shown. The cross symbol on the left (at the bottom) denotes the point with maximum allowed  $r$ .

the latter is significantly smaller, the depletion being caused by the absence of trilinear couplings of  $A^0$  with the charged Higgs bosons. Furthermore, we wish to emphasize the existence of a region of parameter space where  $\langle \sigma_{\gamma\gamma \rightarrow H^0} \rangle$  and  $\langle \sigma_{\gamma\gamma \rightarrow h^0} \rangle$  can both be simultaneously sizeable. That region (e.g. for Set I) is just the allowed domain in the down-right corner in Fig. 5. There we find  $\langle \sigma_{\gamma\gamma \rightarrow H^0} \rangle \simeq 0.2$  pb and  $\langle \sigma_{\gamma\gamma \rightarrow h^0} \rangle \simeq 0.05$  pb, entailing some  $10^4 - 10^5$  events within the standard luminosity range. This possibility can be very relevant, as it could be responsible for a potentially distinctive 2HDM signature which is unmatched in the MSSM.

We have also tested the enhancement potential of the 2HDM in the domains of parameter space where the 3H-coupling (15) is not relevant and where the bulk of the contribution concentrates on the Higgs-fermion Yukawa couplings in combination with the gauge bosons. In the case of generic type-II models, there is no enhancement at large  $\tan \beta$  (unlike the supersymmetric case) inasmuch as  $\tan \beta$  is severely constrained by unitarity. In general, due to the destructive interference between the diagrams dominated by the 3H-coupling and the rest (fermion and gauge boson loops), the enhancement capabilities of the Yukawa sector become overshadowed. As a consequence, in such region we meet the following situation: 1) There are still non-negligible domains in the 2HDM parameter space where the cross-section departs remarkably from its SM counterpart. However, in most cases the departure entails a significant (e.g. 10%) reduction of the cross-section with respect to the SM; 2) type-I and type-II models become essentially indistinguishable in that domain. This is a reflect of the fact that the Higgs-top quark coupling (which has the same form in either type-I and type-II models) drives the leading contribution in the Yukawa sector, whereas the gauge boson contribution is common in both types of models. Therefore, spotting a tail of non-SM effects in this region could not distinguish the type of 2HDM. Still, the missing number of events could certainly hint at the existence of a smoking gun triggered by physics beyond the SM.

Let us close this section by briefly mentioning that we have also surveyed the impact of another, more restrictive, set of unitarity constraints [21]. We have found that, in the most optimistic scenario for  $h^0$  production in  $\gamma\gamma$  collisions, the  $H^+H^-h^0$  coupling lies roughly a factor 2 – 3 below the largest value it can take under the current set of constraints (1) and (2). Correspondingly, the enhancement with respect to the SM would be a factor 5 – 10 times milder, thus dwarfing the

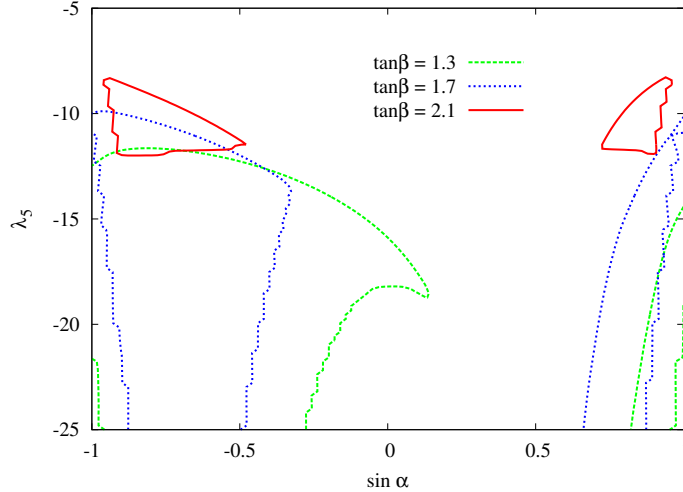


Figure 6: Regions in the  $(\lambda_5, \sin \alpha)$  plane (allowed by all the constraints) where the ratio (17) is  $r > 1.1$ , i.e. when  $g_{\gamma\gamma h}$  is at least 10% bigger than  $g_{\gamma\gamma H}$  for  $\tan \beta = 1.3, 1.7$  and  $2.1$

relevance of the main effects in some regions of the parameter space. We point out, though, that the unitarity restrictions proposed in [21] are not fully coincident with those considered in [22], and in this sense there is still some controversy in the literature on this issue.

## 4 Single Higgs boson production through $\gamma\gamma$ fusion

The interest on virtual photon-fusion (“two-photon processes”) certainly has a long and widespread history in Particle Physics. For instance, a prospect for the measurement of the pion lifetime from

$$e^+e^- \rightarrow \gamma^*\gamma^* \rightarrow e^+e^- + \pi^0 \quad (19)$$

was first discussed by F. Low almost half a century ago [27]. Studies of these processes, as well as detailed considerations on two-photon production of muon pairs and multi-pion final states, were carried out subsequently in the seventies [28]. Remarkably enough, long after the first pioneering studies appeared, two-photon processes are still an active and fruitful field of investigation, in particular for Higgs boson production. In actual fact, single Higgs boson production is, in a sense, the modern counterpart of Low’s “single-meson” production from quasi-real two-photon collisions. Already in the early eighties, this Higgs production channel was first studied in the literature within the context of the old  $e^+e^-$  (pre-LEP) colliders by Grifols and Pascual [15].

To be sure, the traditional two-photon processes are the forerunner of the future  $\gamma\gamma$  colliders considered in the previous section. These colliders will probably concentrate most of the interest around linac physics in the future and may greatly supersede the former in all practical searches for new physics. It is instructive to see once more why, specially in regard to the “Higgs issue”, a most sensitive matter these days. To this end, we compute here the cross-section for the processes

$$e^+e^- \rightarrow \gamma^*\gamma^* \rightarrow e^+e^- + h \quad (h = h^0, H^0, A^0), \quad (20)$$

and compare with the results for real  $\gamma\gamma$  collisions studied in the previous section. In practice, we concentrate on the lightest CP-even state. Noteworthy is the fact that the cross-section for the virtual  $\gamma^*\gamma^*$ -fusion processes, in contradistinction to the real  $\gamma\gamma$  collisions, grows with the CM energy up to very high values of  $\sqrt{s}$ . Generically, the behavior of  $e^+e^- \rightarrow \gamma^*\gamma^* \rightarrow Y + e^+e^-$  in

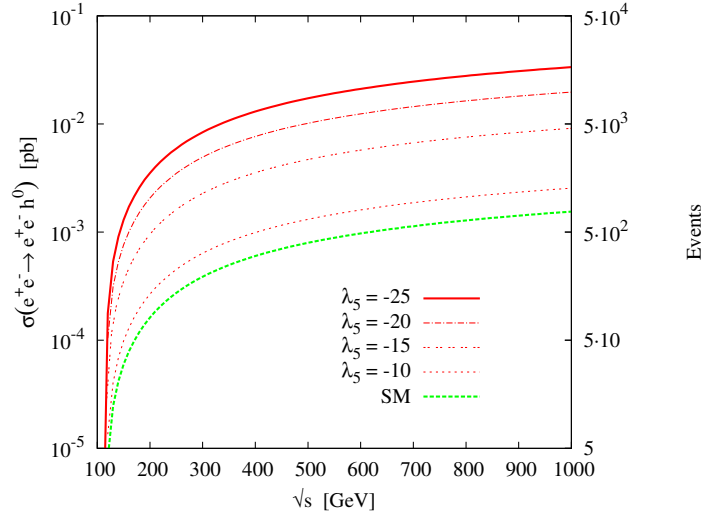


Figure 7: Evolution of the two-photon cross-section  $\sigma(e^+e^- \rightarrow e^+e^-h^0)$  as a function of the CM energy and the corresponding number of events for a total luminosity  $\mathcal{L} = 500 \text{ fb}^{-1}$ . We include the 2HDM and SM curves using the Set I mass parameters,  $\sin \alpha = -0.86$ ,  $\tan \beta = 1.7$  and four values of  $\lambda_5$ .

the asymptotic energy regime goes as  $\sim (\alpha^4/M^2) \ln^2(s/m_e^2) \ln^n(s/M^2)$ , where  $M$  is the threshold mass of the produced final state  $Y$ , and the number  $n \geq 1$  depends on the high energy behavior of  $\sigma(\gamma\gamma \rightarrow Y)$ . The logarithmic growth simply tracks the dynamical feature that, for these processes, the virtual photons  $\gamma^*$  can be quasi-real and hence have their momenta well-below the CM energy of the process, which may satisfy  $s \gg M_V^2$  – the rest of the energy being carried away by the concomitant lepton final states. Recently, the pairwise production of Higgs-bosons via weak gauge-boson fusion mechanism,  $e^+e^- \rightarrow V^*V^* \rightarrow hh + X$  ( $V = W^\pm, Z$ ;  $h = h^0, H^0, A^0, H^\pm$ ) was analyzed in Ref. [7] at the leading order  $\mathcal{O}(\alpha_{ew}^4)$ . The process turned out to be instrumental for probing the 3H self-interactions. A complementary strategy along the same lines is offered by the  $\gamma\gamma$ -fusion process (20), in which the loop-induced  $\gamma\gamma h$  vertex at order  $\mathcal{O}(\alpha_{em}^4 \alpha_{ew})$  can be dominated by the 3H coupling.

The technical complications associated to two-photon processes of the kind (19)-(20) were tackled long ago in the literature (cf. [28] for a classical review). The physics is also well understood, it boils down to the well-known *equivalent-photon or Weizsäcker-Williams approximation*, by which the virtual photon emitted from the scattered electron appears near the mass shell. This feature allows to essentially trade the process of electro-production for a photo-production one with an appropriate photon spectrum. The so-called *photon* content of a given electron can be explicitly factorized and the production cross-section can be approximated in the following way:

$$\sigma(e^+e^- \rightarrow e^+e^-X) = \left[ \frac{\alpha_{em}}{2\pi} \log \left( \frac{s}{4m_e^2} \right) \right]^2 \int_{\tau_0}^1 f(\tau) \sigma_{\gamma\gamma \rightarrow X}(\tau s) d\tau, \quad (21)$$

where  $\tau_0 \equiv M_X^2/s$  and  $f(\tau) = (1/\tau) [(2+\tau)^2 \log(1/\tau) - 2(1-\tau)(3+\tau)]$ .

Figure 7 presents the logarithmic evolution of the production cross-section  $\sigma(e^+e^- \rightarrow e^+e^-h^0)$  as a function of the CM energy. We have used the mass Set I and the optimal parameters quoted in Table 2. Once the production threshold has been surpassed, the cross-section suddenly increases up to a value of about  $10^{-2} \text{ pb}$  and becomes persistently sustained, with only a mild (logarithmic) evolution. Over this approximate plateau, it amounts to more than 5000 events for an integrated luminosity  $\mathcal{L} = 500 \text{ fb}^{-1}$ , therefore resulting in an enhancement of one order of magnitude with respect to the SM. Even more remarkable is the fact that, despite the fairly large value of the

two-photon cross-section, it is still a factor of 10 (at least) smaller than that of the corresponding  $\gamma\gamma$  real scattering processes, for the same values of the 2HDM parameters (cf. Fig 3). This should explain vividly and convincingly the outstanding superiority of the future  $\gamma\gamma$  colliders versus the ancient two-photon processes.

## 5 Conclusions

We have devoted this work to analyze the production of a single neutral Higgs boson,  $h = h^0, H^0, A^0$ , within the two-Higgs-doublet model (2HDM) through the following complementary mechanisms: i) direct scattering of real photons in a  $\gamma\gamma$  collider; and ii) fusion of a virtual photon pair in a conventional two-photon process,  $e^+e^- \rightarrow e^+e^-\gamma^*\gamma^* \rightarrow e^+e^- + h$ . Both mechanisms are direct handles on the effective  $\gamma\gamma h$  interaction,  $g_{\gamma\gamma h}$ . This coupling is a pure quantum effect generated by a plethora of radiative corrections involving charged Higgs bosons, quarks and gauge bosons. Among the interactions in the loops, we have the 3H self-interactions, most remarkably  $H^+H^-h^0$  in the case of  $h^0$  production – which proves to be utterly dominant in certain regions of the 2HDM parameter space. We have systematically swept this space and identified those configurations for which the departure from the SM prediction is most remarkable, and we have done this in full compliance with the rigorous constraints dictated by perturbativity, unitarity and vacuum stability bounds, as well as by the EW precision data. The result is that, in the most favorable scenarios, the physical cross-section (i.e. the one convoluted with the backscattered luminosity function) can typically reach the level of  $\langle\sigma_{\gamma\gamma\rightarrow h}\rangle \sim 0.1 - 1$  pb. In other words,  $\langle\sigma_{\gamma\gamma\rightarrow h}\rangle$  may rocket to values 10 – 100 bigger than the expected SM yield  $\langle\sigma_{\gamma\gamma\rightarrow H}\rangle$  (for similar values of the Higgs mass), which by itself should already be perfectly measurable:  $\langle\sigma_{\gamma\gamma\rightarrow H}\rangle \sim 0.01$  pb = 10 fb. Such notorious enhancement can be traced back to the behavior of the  $H^+H^-h^0$  coupling, despite it is highly restrained by the overall constraints. By sticking to moderate  $\tan\beta \gtrsim 1$ , it is possible to licitly increase the rates by choosing relatively large (negative) values of the parameter  $\lambda_5$ . Moreover, in order to optimize this mechanism, the charged Higgs boson should be relatively light (say, below 300 GeV) so that the associated quantum corrections are not severely hampered by the decoupling effects. It means that the  $g_{\gamma\gamma h}$ -enhancements that we have encountered do strictly apply only for type-I 2HDM, because for this kind of models the mass of the charged Higgs boson is not constrained by  $\mathcal{B}(b \rightarrow s\gamma)$ . A similar conclusion ensues for the case of double Higgs production in  $\gamma\gamma$  collisions, but with lower cross-sections [14].

In the above conditions, the expected number of single Higgs boson events emerging from direct  $\gamma\gamma \rightarrow h$  scattering, within the typical energy range of the ILC (500 – 1000 GeV), is of the order of  $10^5$  per 500 fb $^{-1}$  of integrated luminosity. Compared to the production rate of single Higgs bosons through the traditional virtual photon-pair fusion,  $e^+e^- \rightarrow e^+e^-\gamma^*\gamma^* \rightarrow e^+e^- + h$  (which performs at the level of 0.01 pb, at most, for  $\sqrt{s} \geq 500$  GeV), the real  $\gamma\gamma$ -collision mechanism is at least one order of magnitude more efficient.

On the experimental side, the prospects for Higgs boson detection in a  $\gamma\gamma$ -collider are deemed to be excellent. To start with, let us stress that the single Higgs-boson final state is to be produced essentially at rest. Therefore, for  $M_h < 2M_V \lesssim 180$  GeV, the corresponding signatures should mostly be in the form of back-to-back, highly energetic, quark jets ( $b\bar{b}, c\bar{c}$ ). For  $M_h > 2M_V$ , instead, signatures with two or four charged leptons in the final state (from  $W^\pm \rightarrow \ell^\pm +$  missing energy and, specially, from  $Z \rightarrow \ell^+\ell^-$ ) should be really pristine. Furthermore, we have seen that, in some cases, the two channels  $\gamma\gamma \rightarrow h^0$  and  $\gamma\gamma \rightarrow H^0$  are simultaneously accessible and with similar rates. Needless to say, this could result in a double distinctive signature of new physics.

With enough statistics on these events, and upon analyzing the invariant mass distribution of the resulting jets of quarks and leptons, the measurement of some 2HDM Higgs boson(s) mass(es) should be attainable with fairly good accuracy, together with a precise determination of the effective

$g_{\gamma\gamma h}$  couplings (typically for  $h^0$  and/or  $H^0$ ). If their strengths would happen to be vastly dominated by the triple Higgs boson self-interactions, the signature of non-standard Higgs boson physics would be crystal-clear, leading us to suspect it to be rooted in some generic type-I 2HDM. However, should we meet the juncture  $g_{\gamma\gamma h} \lesssim g_{\gamma\gamma H}$  or  $g_{\gamma\gamma h} \gtrsim g_{\gamma\gamma H}$ , the underlying quantum effects would be largely insensitive to the type of model and a detailed comparative study with the MSSM would be mandatory [29]. Even then, tiny deviations could hint at new physics. In this regard, it is important to emphasize that, given the high precision nature of a  $\gamma\gamma$  collider, gathering a small 5 – 10% effect (positive or negative) should be sufficient to point at a smoking gun.

To summarize, a  $\gamma\gamma$  collider should be the natural arena for high precision Higgs boson experiments. After producing one or more Higgs bosons and performing an accurate determination of the effective coupling(s)  $g_{\gamma\gamma h}$ , we should find ourselves in a vantage point to successfully carry the architecture of the Electroweak Symmetry Breaking through to completion.

**Acknowledgments** JS is grateful to F. Mescia for useful discussions on the bounds on the charged Higgs boson mass from low energy physics. NB thanks an ESR position of the EU project RTN MRTN-CT-2006-035505 Heptools; DLV acknowledges the MEC FPU grant AP2006-00357. DLV and JS have been supported in part by MEC and FEDER under project FPA2007-66665 and by DURSI Generalitat de Catalunya under project 2005SGR00564. This work was partially supported by the Spanish Consolider-Ingenio 2010 program CPAN CSD2007-00042.

## References

- [1] H.P. Nilles, *Phys. Rept.* **110** (1984) 1; H.E. Haber, G.L. Kane, *Phys. Rept.* **117** (1985) 75.
- [2] J.F. Gunion, H.E. Haber, G.L. Kane and S. Dawson, *The Higgs hunter's guide*, Addison-Wesley, Menlo-Park, 1990.
- [3] D. Garcia and J. Solà, *Mod. Phys. Lett.* **A9**, 211 (1994); P.H. Chankowski, A. Dabelstein, W. Hollik, W. M. Mosle, S. Pokorski, J. Rosiek, *Nucl. Phys.* **B417** (1994) 101; D. Garcia, R. A. Jiménez and J. Solà, *Phys. Lett.* **B347** (1995) 309; *Phys. Lett.* **B347** (1995) 321.
- [4] J. A. Coarasa, D. Garcia, J. Guasch, R. A. Jiménez, J. Solà, *Eur. Phys. J.* **C2**, 373 (1998); *Phys. Lett.* **B425** (1998) 329; R. A. Jiménez, J. Solà, *Phys. Lett.* **B389** (1996) 53; J.A. Coarasa, R. A. Jiménez, J. Solà, *Phys. Lett.* **B389** (1996) 312; J. Guasch, R.A. Jiménez and J. Solà, *Phys. Lett.* **B360** (1995) 47.
- [5] S. Heinemeyer, *Higgs Physics at the LHC: Some Theory Aspects*, arXiv:0807.2514 [hep-ph]; A. Djouadi, *The Higgs sector of supersymmetric theories and the implications for high-energy colliders*, arXiv:0810.2439 [hep-ph]; A. Djouadi, R.M. Godbole, *Ewsb at LHC*, arXiv:0901.2030 [hep-ph]; A. Djouadi, *Phys. Rept.* **457** (2008) 1; *Phys. Rept.* **459** (2008) 1.
- [6] G. Ferrera, J. Guasch, D. López-Val, J. Solà, *Phys. Lett.* **B659** (2008) 297; arXiv:0801.3907.
- [7] R.N. Hodgkinson, D. López-Val, J. Solà, *Phys. Lett.* **B673** (2009) 47.
- [8] *ILC Reference Design Report Volume 2: Physics at the ILC*, arXiv:0709.1893 [hep-ph]; *Physics interplay of the LHC and the ILC*, (G. Weiglein *et al.*), *Phys. Rept.* **426** (2006) 47.
- [9] A. Djouadi, W. Kilian, M. Mühlleitner and P.M. Zerwas, *Eur. Phys. J* **C10** (1999) 27. For tree-level double Higgs production processes, see e.g. the exhaustive overview by M. Mühlleitner, hep-ph/0008127.



- [10] A. Djouadi, H.E. Haber and P.M. Zerwas, *Phys. Lett.* **B375** (1996) 203; A. Djouadi, V. Driesen, W. Hollik and J. Rosiek, *Nucl. Phys.* **B491** (1997) 68.
- [11] P. Osland and P.N. Pandita, *Phys. Rev.* **D59** (1998) 055013; D.J. Miller and S. Moretti, *Eur. Phys. J* **C13** (2000) 459; F. Boudjema and A. Semenov, *Phys. Rev.* **D66** (2002) 095007.
- [12] A. Arhrib, R. Benbrik, C.-W. Chiang, *Phys. Rev.* **D77** (2008) 115013, arXiv:0802.0319; A. Arhrib, W. Hollik, S. Penaranda, M. Capdequi Peyranere, *Phys. Lett.* **B579** (2004) 361.
- [13] See e.g. V. I. Telnov, *Nucl. Phys. Proc. Supp.* **184** (2008) 271; *Acta Phys. Pol.* **B 37** (2006) 1049; A. de Roeck, *Nucl. Phys. Proc. Supp.* **179-180** (2008) 94-103; B. Badelek *et al.*, *Int. J. of Mod. Phys.* **A 19** (2004) 5097.
- [14] F. Cornet and W. Hollik, *Phys. Lett.* **B669** (2008) 58; E. Asakawa, D. Harada, S. Kanemura, Y. Okada and K. Tsumura, arXiv:0809.0094 [hep-ph]; arXiv:0902.2458 [hep-ph]; A. Arhrib, R. Benbrik, C.H. Chen, R. Santos, arXiv:0901.3380 [hep-ph]; L. J. Dixon, Y. Sofianatos, *Phys. Rev.* **D79** (2008) 033002; R. Martínez, J.Alexis Rodríguez and D. Milanés, *Phys. Rev.* **D72** (2005) 035017.
- [15] J.A. Grifols, R. Pascual, *Z. Phys.* **C6** (1980) 353.
- [16] G.V. Jikia, *Nucl. Phys.* **B412** (1994) 57; R. Belusevic, G. Jikia, *Phys. Rev.* **D70** (2004) 073017.
- [17] B. Grzadkowski, J.F. Gunion, *Phys. Lett.* **B294** (1992) 361; J. F. Gunion, H.E. Haber, *Phys. Rev.* **D48** (1993) 5; D.L. Borden, D.A. Bauer, D.O. Caldwell, *Phys. Rev.* **D48** (1993) 4018; M. Mühlleitner, M. Krämer, M. Spira, P. Zerwas, *Phys. Lett.* **B508** (2001) 311; D. M. Asner, J. B. Gronberg, J.F. Gunion, *Phys. Rev.* **D67** (2003) 035009; M. Krawczyk, hep-ph/0307314; P. Niezurawski, A.F. Zarnecki and M. Krawczyk, *Acta Phys. Polon.* **B 37** (2006) 1187.
- [18] A.W El Kaffas, P. Osland, *Phys. Rev.* **D76** (2007) 095001.
- [19] M. Misiak *et al.* *Phys. Rev. Lett.* **98** (2007) 022002.
- [20] Particle Data Group (C. Amsler *et al.*), *Phys. Lett.* **B667** (2008) 1.
- [21] S. Kanemura, T. Kubota and E. Takasugi, *Phys. Lett.* **B313** (1993) 155; A. G. Akeroyd, A. Arhrib and E.-M. Naimi, *Phys. Lett.* **B490** (2000) 119.
- [22] J. Horejsi and M. Kladiva, *Eur. Phys. J* **C46** (2006) 81.
- [23] B.W. Lee, C. Quigg, H.B. Thacker, *Phys. Rev. Lett.* **38** (1977) 883; *Phys. Rev.* **D16** (1977) 1519.
- [24] S. Kanemura, T. Kasai and Y. Okada, *Phys. Lett.* **B471** (1999) 182.
- [25] T. Hahn, *FeynArts 3.2*, *FormCalc* and *LoopTools* user's guides, available from <http://www.feynarts.de>; T. Hahn, *Comput. Phys. Commun.* **168** (2005) 78.
- [26] V. I. Telnov, *Acta Phys. Polon.* **B 37** (2006) 633; A. F. Zarnecki, *Acta Phys. Polon.* **B34** (2003) 2741.
- [27] F. Low, *Phys. Rept.* **120** (1960) 582.
- [28] H. Terazawa, *Rev. Mod. Phys.* **45** (1973) 615.
- [29] N. Bernal, D. López-Val, J. Solà, work in progress.